Fast Capture of Spectral Image Series

Sebastian Merzbach[1], Michael Weinmann[1], Martin Rump[2] and Reinhard Klein[1]
[1]*Institute of Computer Science II, University of Bonn, Friedrich-Ebert-Allee 144, Bonn, Germany*
[2]*X-Rite, Inc., 4300 44th St. SE, Grand Rapids, U.S.A.*

Keywords: Spectral, Reflectance, Noise, Spectral Reconstruction.

Abstract: In recent years there has been an increasing interest in multispectral imaging hardware. Among many other applications is the color-correct reproduction of materials. In this paper, we aim at circumventing the limitations of most devices, namely extensive acquisition times for acceptable signal-to-noise-ratios. For this purpose we propose a novel approach to spectral imaging that combines high-quality RGB data and spatial filtering of extremely noisy and sparsely measured spectral information. The capability of handling noisy spectral data allows a dramatic reduction of overall exposure times. The speed-up we achieve allows for spectral imaging at practical acquisition times. We use the RGB images for constraining the reconstruction of dense spectral information from the filtered noisy spectral data. A further important contribution is the extension of a commonly used radiometric calibration method for determining the camera response in the lowest, noise-dominated range of pixel values. We apply our approach both to capturing single high-quality spectral images, as well as to the acquisition of image-based multispectral surface reflectance. Our results demonstrate that we are able to lower the acquisition times for such multispectral reflectance from several days to the few hours necessary for an RGB-based measurement.

1 INTRODUCTION

The generation of photo-realistic images is a central requirement for many applications in computer graphics. Especially visual prototyping relies on the the correctness of the generated images as design decisions are usually based on computer-generated images. But also applications in the entertainment and advertisement industry benefit from color-correct depictions of 3D content. For this reason, it is not surprising that measuring real light and reflectance has become a standard approach in many industrial applications. While the traditionally used RGB capturing devices suffer from a bad color reproduction due to metamerism effects, a color-correct rendering can only be achieved using light and reflectance spectra with a higher resolution than the three broad-band channels in RGB-based devices.

The main limitation that prevents spectral measurements from a widespread use in graphics are the still very high costs of multispectral snapshot cameras. An alternative would be the use of conventional, cheaper spectral cameras, which distribute the acquisition effort for the separate spectral bands into the temporal domain using e.g. filter wheels or tunable filters. However, the acquisition effort does not scale linearly with the number of spectral bands, as some of these bands require much higher exposure times due to variations in the illumination spectrum and the quantum efficiency of the sensor. This renders these devices unsuitable for many time-critical applications. One such application is multispectral reflectance capturing, where tens of thousands of photos have to be taken of a surface under varying illumination and viewing directions. For RGB-based reflectance acquisition, a significant reduction of the total measurement times in comparison to the sequential gonioreflectometer-based acquisition is usually achieved by a parallelized acquisition using camera arrays (Schwartz et al., 2014). Unfortunately, this strategy is impractical when using snapshot multispectral cameras as the costs of a single spectral camera often exceed those of ten RGB cameras.

To reduce the acquisition times of non-snapshot spectral cameras to practicality, it is therefore desirable to reach the highest possible efficiency for existing hardware, which ultimately requires raising the signal-to-noise-ratio (SNR) for all of the spectral band images. An obvious approach would be simply increasing the light intensity. However, this cannot be

Merzbach S., Weinmann M., Rump M. and Klein R.
Fast Capture of Spectral Image Series.
DOI: 10.5220/0006175901480159
In *Proceedings of the 12th International Joint Conference on Computer Vision, Imaging and Computer Graphics Theory and Applications (VISIGRAPP 2017)*, pages 148-159
ISBN: 978-989-758-224-0

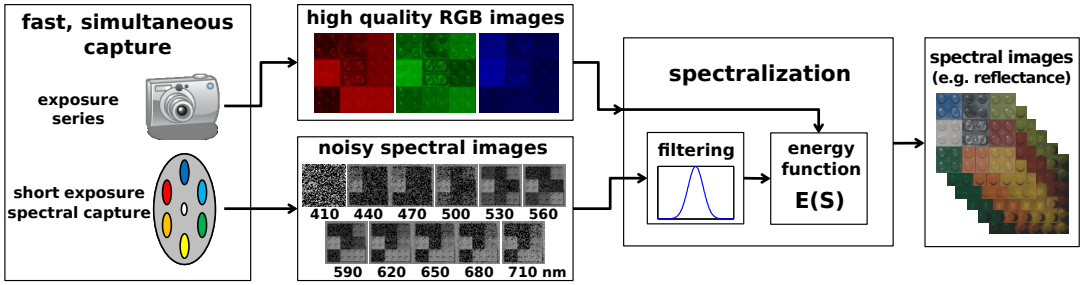

Figure 1: Method overview: We present a spectral reconstruction technique that is able to deal with extremely noisy input data by incorporating high-quality RGB data and filtering on the noisy data in the reconstruction process. Our method is especially well suited for capturing a huge number of similar spectral images which is for example required for reflectance capture. Accepting a high noise level allows to use spectral cameras at much lower exposure times, enabling for a vast speed-up compared to traditional techniques.

easily achieved in all scenarios or acquisition setups.

A class of approaches for multispectral image acquisition relies on reconstructing the full spectral data cubes from a combination of high-quality broadband and sparse narrowband data (Imai and Berns, 1998; Hardeberg et al., 1999; Rump and Klein, 2010). Here, the image is captured using several broadband filters (e.g. RGB) and additional sparse knowledge about spectra in the image is added to guide the reconstruction of dense spectral information. While being conceptually elegant, the *spectralization* method has only been demonstrated on synthetic examples. One reason for this is the need for low noise spectral measurements that result in impractical exposure times. Taking the images with narrow bandpass filters would require long exposure times to have a good signal-to-noise ratio even for high-quality cameras. Furthermore, a pixel-accurate alignment between RGB and sparse spectral data obtained from a line camera is required, which is difficult to achieve.

The approach presented in this paper makes the *spectralization* method applicable for image-based multi-spectral reflectance acquisition and enables the reconstruction of the full spectral data from high-quality RGB and noisy spectral data. To keep the acquisition times low, we allow high noise levels in the spectral data and counteract the noise by spatial filtering. We use a monochrome CCD camera together with a tunable bandpass filter (see (Hardeberg et al., 2002)) for imaging distinct spectral bands. An overview of our approach is illustrated in Figure 1. Using our method, spatially varying, bi-angular, spectral reflectance can be captured roughly at the speed of RGB reflectance. In addition, our technique can easily be integrated into existing RGB measurement setups without the need of integrating stronger light sources or other dedicated hardware except for one spectral camera. We realized a respective measurement setup and used it to evaluate the reconstruction quality and performance of our method.

Moreover, we show how to obtain an exact radiometric and spectral calibration of cameras when operated at a bad SNR. Due to the narrow band filters and the enforced short exposure times, our spectral camera operates at intensity ranges which are very close to the noise level. To be able to extract radiometrically calibrated data from the captured images, we need to extend the camera response curve with high accuracy even at those low intensities. This is usually a range which is completely excluded by weighting schemes from reconstruction methods. We show how to preprocess the data close to the camera's noise level, so that we can obtain meaningful calibration data from one such method (Robertson et al., 2003), enabling us to use these corrupted images as input to our spectral reconstruction method.

The key contributions of our novel approach can be summarized as follows:

- the practical spectral reflectance capture: the extension of the spectralization method allows for low exposure times for single spectral bands, and thus, for a speed-up of spectral BTF acquisition to measurement times comparable to the ones of RGB setups,
- the possibility to re-use existing RGB setups by simple addition of one or a few spectral cameras, no need to increase power of illumination or change the device geometry,
- the radiometric calibration of cameras operating at low pixel values.

2 RELATED WORK

Almost all conventional approaches for capturing multispectral images involve scanning either through the spectral domain using tunable filters or filter

wheels, or scanning in the spatial dimension. This scanning dramatically increases the acquisition times, which becomes particularly noticeable in applications such as bi-angular reflectance capture where tens of thousands of photos have to be taken. Other methods rely on reconstruction algorithms, which are often sensitive to noise and therefore produce unreliable results in scenarios where the illumination cannot be increased but short acquisition times are necessary. Shrestha and Hardeberg compared and evaluated several such multispectral cameras (Shrestha and Hardeberg, 2014). This comparison shows that there is no camera hardware that combines a high spectral *and* spatial resolution with short acquisition times. Though there are spectral cameras which allow for a snapshot acquisition like RGB cameras, these devices suffer from limited spatial resolution and light sensitivity because the spectral information is spread over the spatial domain by optical elements. An exhaustive survey of spectral snapshot cameras has recently been performed (Hagen and Kudenov, 2013). In summary, snapshot spectral cameras are not only extremely expensive, but they also rely on bright light sources to account for their limited light sensitivity.

Multispectral Reflectance Acquisition. Converting gonioreflectometers from RGB to multispectral is straightforward. However, due to the serial nature of the capture process, filter switching and long exposure times necessary for high-quality spectral images, the measurement times are impractically high. Nevertheless, such brute-force measurements have already been conducted. Tsuchida et al. (Tsuchida et al., 2005) used a monochrome camera and placed a wheel with 16 different bandpass-filters in front of the light source. Rump et al. (Rump et al., 2010) placed a liquid crystal tunable filter in front of a monochrome camera, achieving a spectral resolution of 32 bands. Unfortunately, both setups are impractically slow, as the measurement times are on the order of days.

Hybrid Methods. The following techniques are based on the combination of high-quality RGB measurements and sparse spectral measurements (Imai and Berns, 1998; Hardeberg et al., 1999; Rump and Klein, 2010). The great advantages of hybrid methods are the high spatial resolution and the re-use of existing RGB technology. Sparse spectral information of images can e.g. be acquired by using a line-scanning spectral camera (Rump and Klein, 2010). Unfortunately, it is a serious problem to spatially register 2D RGB images and the 1D spectral line for arbitrary scene geometry. When no additional knowledge about the imaged spectra is present, the pseudoinverse of the RGB filter matrix can be applied (Imai and Berns, 1999), typically resulting in a bad reconstruction. A much better inverse matrix can be set up (Hardeberg et al., 1999) as soon as additional knowledge about spectra is present. Unfortunately, the methods based on inverse matrices map all measured values to a three-dimensional hyperplane in the spectral space. This leads to errors as soon as multiple materials are present in the scene. This limitation can be removed by casting the spectral reconstruction as an optimization problem (Rump and Klein, 2010). While this technique has proven to give excellent results when applied to complex images, several problems render it impractical: It requires low noise spectral data, resulting in impractical exposure times, and with their setup the authors rely on a pixel-accurate alignment of 2D RGB images and a 1D spectral scanline. We also propose the use of a hybrid method. Instead of a spectral line camera, we use a monochrome CCD camera together with a tunable bandpass filter (see (Hardeberg et al., 2002)) for imaging distinct spectral bands. This 2D spectral data can be accurately aligned with the 2D RGB data. An additional spatial filtering makes our method capable of handling high noise levels in the spectral data. As demonstrated by our results, we can reconstruct the full spectra from high-quality RGB and noisy spectral data.

Image Denoising. There are several methods that try to denoise photographs taken under poor lighting conditions. These approaches are similar to the one proposed in this paper as they all use additional imaging modalities to guide the denoising. Where our method uses high quality RGB images to improve low quality spectral images, these methods all make use of high quality flash images to improve noisy images taken under low light conditions. Petschnigg et al. (Petschnigg et al., 2004) combine a sequence of flash and no-flash images to transfer detail from the well-exposed flash- to the noisy image. To do so, they apply a joint bilateral filter on the two images. Additionally, they have to deal with shadows and highlights caused by the flash to avoid artifacts in the denoised image. Matsui et al. (Matsui et al., 2009) allow to capture both images at the same time by using a near infrared (NIR) flash that does not interfere with the no-flash image. After applying a joint bilateral filter, they additionally extract a “detail image” that contains noise and fine detail that was lost due to the filtering. They remove the noise by applying a joint non-local mean to the detail image and can use it to restore the fine scale structures in the filtered photograph. By computing a blur kernel via optical flow on a sequence of NIR-flash images, they are even able to

remove motion blur from a noisy image via deconvolution. In 2009, Krishnan and Fergus (Krishnan and Fergus, 2009) approached the problem in a different manner: They also improve a low light ambient image by a "dark" flash image, which they realize by blocking the visible part of the flash spectrum. In contrast to previous methods they minimize an energy function that rewards a reconstruction close to the colors observed under ambient light while having similar gradients as the dark flash image. Takeuchi et al. (Takeuchi et al., 2013) again use an NIR-flash, but instead perform a decorrelation of luminance and chroma information. The chroma information is taken from a denoised no-flash image, whereas the luminance is estimated from the flash image by predicting the spectral response in RGB. These methods are certainly applicable for denoising multispectral images by using high quality RGB instead of the flash images. However, they all lack the flexibility that we can exploit with our energy function formulation with regard to sparsely and incompletely measured spectral band images. The existing work requires dense correspondences for all image modalities (flash / no-flash), whereas our method allows for "missing" spectral bands for some of the RGB images. These missing correspondences are compensated for by our regularization over an appearance neighborhood.

3 SPECTRAL RECONSTRUCTION

In this section, we introduce our novel method that is able to reconstruct full spectral images from high-quality RGB data and noisy spectral data.

We suggest to utilize a monochrome camera with tunable bandpass filter at low exposure times. This produces images with high spatial resolution but a very low SNR. However, this configuration has the fundamental advantage that a pixel-accurate alignment between RGB and band-filtered images is possible. One way to register the images would be to use a common optical path and a beam splitter. Another, much simpler option would be to register both cameras in beforehand, if a series of spectral bands have to be imaged with non-changing geometry. In the latter case, the spectral camera system can be registered by taking one image with long exposure time in beforehand which then allows for registration against the RGB images using markers or standard methods like optical flow. This second technique is especially useful for reflectance measurements because, in this case, huge image series have to be captured where only changes in lighting occur.

Of course, the noisy band-filtered images cannot be used directly. To get rid of the noise in the single band-filtered images, filtering is necessary which leads to a loss of high frequent spatial details. Fortunately, the low-noise and high-resolution RGB images should provide enough information to recover those details. Imai and Berns (Imai and Berns, 1998) also proposed to capture with different spatial resolutions, and to reconstruct the high-resolution spectral image afterwards. However, they also stick to a low dimensional subspace of the spectral space and only aim at reconstructing $L^*a^*b^*$ images. In contrast, we would like to reconstruct a full spectral image and do not want to accept limitations on the dimensionality of the imaged spectra. Our energy function is inspired by the one used by Rump and Klein (Rump and Klein, 2010). We incorporate the filtering directly into the energy function by ensuring that the filter response to the unknown target image matches the filter response on the noisy input images. Then, the optimizer is responsible for finding a solution which respects both high frequent details and low frequent spectral information.

The new principle leads to the following energy function:

$$\begin{aligned} E(S) &= \alpha \sum_{i=1}^{K} \left\| \sum_{p=1}^{P} F_i(p)\,(S_{b_i}(p) - D_{b_i}(p)) \right\|^2 \\ &+ \beta \sum_{p=1}^{P} \|\mathbf{C}S(p) - R(p)\|^2 \\ &+ \gamma \sum_{p=1}^{P} \sum_{n \in N_p} \|S(p) - S(n)\|^2 \end{aligned} \tag{1}$$

Here, p denotes a pixel position, P the total number of all pixels, K is the number of spatial filters applied to the data and α, β and γ represent weights for the individual terms. The first term ensures that applying a spatial filter F_i to the unknown band-filtered image S_{b_i} matches the filter response on the noisy, measured image D_i of the same waveband. The b_i select the respective wavelength band corresponding to the i-th filter kernel. The second and third term are similar to the ones in the work of Rump and Klein (Rump and Klein, 2010). The matrix $\mathbf{C}$ contains the RGB camera's spectral sensitivity curves in its rows. It is used to convert the unknown spectra S to RGB to enforce a similarity to the measured RGB data R. To make the problem tractable, we further regularize over a similarity in an appearance neighborhood N_p. The neighborhood N_p for pixel p is determined as a fixed number of closest pixels in a user-selected appearance space. As it is straight forward and provides good results, we compute N_p as the k nearest neighbors in the camera's RGB space with $k = 3$.

Filtering. To reduce the noise level in the spectral data, Gaussian filters are used. We chose Gaussian filters to make the method more robust w.r.t. small misalignments in the registration of the spectral and RGB images. If in contrast the noise was removed by averaging the pixel values in a fixed neighborhood, i.e. if we had applied simple box filters, only small misalignments in the registration would introduce a strong bias in the reconstruction. The size of the individual filters is adapted to the noise level in the different wavebands. These noise levels depend on the quantum efficiencies and on the chosen exposure times of the single spectral bands. The exposure times were chosen as

$$t_i = \left(\frac{t_0}{Q_i \cdot L_i} \right)^{\omega}, \tag{2}$$

where t_0 is a constant, Q_i is the camera's quantum efficiency at the wavelengths corresponding to the i-th band and L_i is the spectral radiance of the illumination in spectral band i (see Figure 3). The exponent ω can be used as a weight between accepted noise level and time spent for the exposure. In our experiments, we chose $\omega = 0.8$. Thus, spectral bands with high noise levels caused by bad camera sensitivity or weak illumination receive longer exposure times. The filter sizes are then calculated as

$$s_i = \frac{s_0}{Q_i \cdot L_i \cdot t_i}, \tag{3}$$

where s_0 again is a constant. Both t_0 and s_0 solely depend on the hardware and are chosen manually. The exposure times t_i and filter sizes s_i resulting for our camera hardware and light sources can be seen in Figure 3. The standard deviation σ_i of the Gaussian filters is set to $s_i/5$.

Filter Placement. During filtering, only regions *inside* the image boundaries are considered, i.e. the filter centers are positioned with a distance of s_i to the image boundaries. The centers are then placed at least every d pixels, independent of their size. To limit the size of the resulting system of equations and since a pixel-wise convolution would result in many redundant filter responses, we chose $d = 2.5$ in our experiments. This placement still causes heavy overlap of the kernels in image space. However, we let the optimizer deal with the resulting ambiguities. A conservation of high frequency features is guaranteed via constraints provided by the RGB images.

Optimization. As the energy function described in equation (1) contains only least squares distance terms, its derivative is linear with regard to the unknown variables. For this reason, it can be transformed into a set of linear equations $AS = b$ with a very sparse matrix A. We use an iterative conjugate-gradient method to solve the normal equation $A^T AS = A^T b$. The advantage of this solver is, that neither A nor A^T needs to be stored explicitly and we just have to provide two functions that compute a multiplication of the respective matrix with a vector.

The reconstruction quality is directly dependent on a viable choice of the three weights in equation (1). First of all, it is important to note that the three terms of the energy function have significantly different numbers of distance terms. We therefore propose to weight the three terms equally using the total number of equations $M = K + 3P + \sum_{p=1}^{P} |N_p|$:

$$\alpha = \hat{\alpha}\frac{M}{K}, \quad \beta = \hat{\beta}\frac{M}{3P}, \quad \gamma = \hat{\gamma}\frac{M}{\sum_{p=1}^{P} |N_p|}. \tag{4}$$

For the reconstruction of a single image it is sufficient to choose $\hat{\alpha}$, $\hat{\beta}$ and $\hat{\gamma}$ to be one. When multiple images have to be reconstructed and there is less spectral information per image, the regularization needs to be weighted higher to allow for faster convergence. During our experiments, we found that a value of $\hat{\gamma} = 20$ is a good choice. It should be clarified that this just helps to converge faster and is not necessary for good reconstruction results.

Application for Reflectance Acquisition. For a lot of applications multiple spectral images of very similar scenes need to be taken. This includes measurements of materials' reflectance. In this case, it is not necessary to capture a noisy image for each spectral band and every RGB image. The regularization term will "transport" the spectral information between the images and lead to a reconstruction of the full spectrum for each image even if there is only one noisy spectral image per RGB image. In many cases, it is even possible to reconstruct spectra for RGB images without *any* corresponding spectral information at all, as long as the RGB-image content is sufficiently similar to that of the RGB images with corresponding spectral information.

The applicability of our method for reconstructing spectral images for multiple, possibly different RGB images can be seen in the Section 5. For many hardware configurations an exposure time for the spectral camera suffices that is comparable to that of the RGB camera. Effectively, this speeds up spectral imaging to standard RGB imaging.

In the following, we will first describe the hardware and its calibration used throughout our experiments and we will then discuss the results achieved by our method.

4 SETUP AND CALIBRATION

In this section, we describe the hardware setup used for our experiments. We start with some explanations on the original RGB setup and on the additional dedicated hardware required for the spectral data, with supplemental information on the general applicability of our method. Afterwards the calibration of the setup is explained with greater detail.

RGB Measurement Setup. For our experiments both with single images as well as with full reflectance capture, we utilized an existing setup that was custom-built for RGB-based BTF acquisition (Schwartz et al., 2014). The setup has a hemispherical gantry covered with 198 2.5W Barthelme LEDs which can be switched on and off individually. 11 RGB industry video cameras (SVS Vistek 4022) with a resolution of 2048x2048 pixels are integrated into the gantry, forming an arc on one side from the top position down to an elevation angle of 75° measured from the normal. To measure anisotropic materials as well, the sample holder is mounted onto a precision rotation stage which can orient the samples to arbitrary azimuth angles.

Spectral Integration. To capture spectral data, an additional camera has been mounted into the setup. Here, we use a monochrome CCD camera (Photometrics Coolsnap K4) also with 2048x2048 pixels resolution. In the optical path a liquid crystal tunable filter (CRi Varispec VS10) is mounted. This filter allows for extremely fast change of the spectral bandpass. The average bandwidth is about 10nm and the peak wavelength can be tuned from 400 to 720nm covering the visible spectrum. This camera system is mounted at 45° elevation and with 15° azimuthal distance to the RGB camera at the same elevation. This is important since the LEDs are mounted at the gantry with the same distance. After the sample is rotated by 15° the spectral camera captures the same content as the RGB camera before. Using this arrangement, a nearly pixel-correct alignment between spectral and RGB data is possible.

The measurement process works as follows: the sample is rotated to 24 different positions in 15° steps. For every rotation angle, an image is taken by the RGB cameras and the spectral camera using multiple LEDs switched on to have a high quality image in which the sample holder can be detected with subpixel accuracy to have a perfect alignment between the images of the single cameras. Afterwards the LEDs are serially switched on, images are captured, and the respective LED is switched off again. Since the RGB and the spectral camera system are operated simultaneously, and since the spectral camera system is driven at short exposure times, the measurement process is as fast as a traditional RGB measurement using the same setup. Our measurement setup is able to acquire the necessary 32 noisy band-filtered images within the time needed for 10 high quality, high dynamic range RGB images.

For the reconstruction of spatially varying and bi-angular reflectance the multi-image reconstruction is utilized as described in Section 3. From the set of all RGB images of a measurement run, 20 images are iteratively selected of which 10 are from the camera at 45° elevation and the other 10 should cover other elevation angles but similar light directions. This set of 20 images is then reconstructed using our method. To speed up reconstruction, the recovered spectra from the first image set can be used to get a much better initialization for the following image sets. For this purpose, appearance neighborhoods based on the RGB data of the two image sets are calculated and the spectra are transported from the first set to the second set.

Calibration. We performed a careful calibration of the setup. Here, cameras and light sources have to be calibrated geometrically and radiometrically. The reader is referred to the work of Schwartz et al. for an in-depth description of all calibration steps (Schwartz et al., 2014). We focus on the radiometric calibration only, since the geometric calibration is out of the scope of this work.

First of all, we measured the spectrum of our LED light sources using an Ocean Optics USB4000 spectrophotometer. The spectrum is shown in Figure 3. For the cameras two different kinds of calibrations are required: on the one hand a recovery of the opto-electronic conversion function (OECF) to correct for non-linearities in the sensor's response to light and on the other hand a spectral calibration which aims at finding the response efficiency of the optics-camera combinations depending on the wavelength.

Linearizing the response of the RGB cameras is straightforward and was performed using the algorithm of Robertson et al. (Robertson et al., 2003). To obtain the spectral filter matrix C of the RGB cameras, standard methods can be applied as well (Rump et al., 2011). The spectral sensitivity of the RGB cameras is

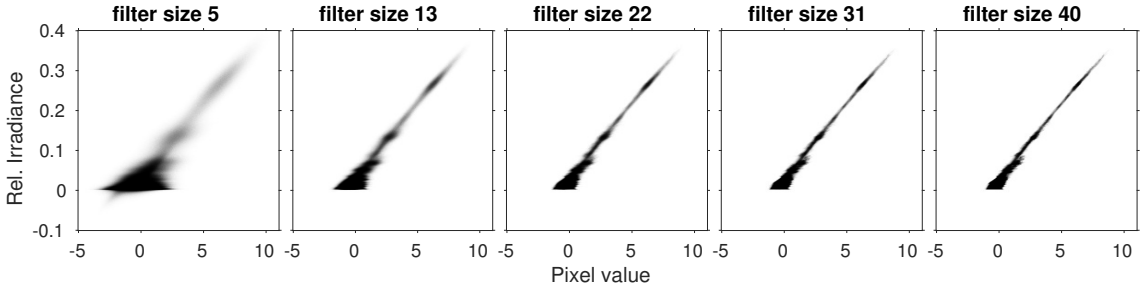

Figure 2: Checking the stability in the bad-SNR range of the monochrome camera: Response histograms on filtered, dark-subtracted (offset by 30) input images after applying Gaussian filters of increasing size. As one can see, negative values after dark-subtraction need to be taken into account since a clipping would bias the result largely. The camera's output in this range is statistically stable despite the fact that the output of the single pixels is shot-noise limited. Due to the stability, data in this pixel value range can be used as an input for our method.

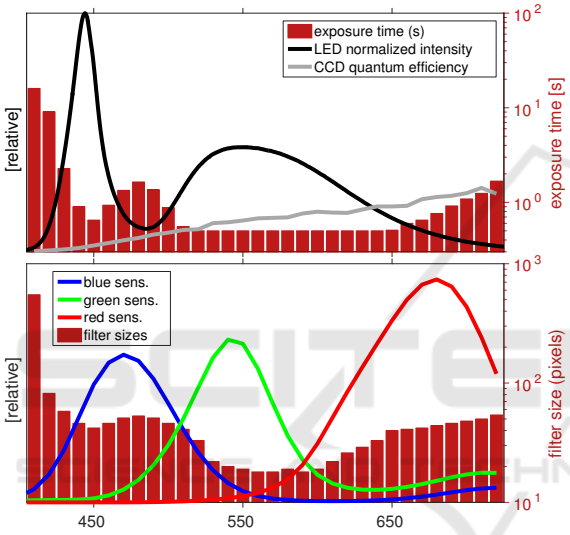

Figure 3: Calibration of the measurement setup. The bar plots show the resulting exposure times (top) and filter sizes (bottom).

shown in Figure 3.

For the spectral camera, much more care has to be taken since here measurements with a very low SNR will be used. Therefore, the calibration of the camera must also hold for low pixels values - a range that is typically excluded using weighting functions. We, however, want to use this range as well because we use largely underexposed band-filtered images as input data. We therefore require a calibration which is exact for the low pixel values, too.

The first step is to obtain exact knowledge about the camera's dark current in all pixels. For this we took 200 photographs with closed shutter and repeated this process for different exposure times. The average over the dark frames is computed with floating point accuracy.

To recover the OECF in the low-pixel-value range, we propose to apply the Robertson algorithm to images modified by dark-subtraction, filtering and a rescaling to the full range of integers corresponding to the camera's bit depth. The filtering is done using a Gaussian kernel as in the spectral recovery method.

As the original algorithm works on discrete integer pixel values, a mapping from the real-valued filtered data has to be applied to obtain integers again. As we take the images with short exposure times, the filtered pixel values all lie in the lower range of the entire interval of valid pixel values. We therefore stretch this small interval to the full length and round these new values to their respective nearest integers. These new integer values can then directly be used in the standard Robertson algorithm.

To show the effect of filtering on response recovery, we computed response histograms for an exposure series having extremely low pixel values. Figure 2 shows the histograms for different filter sizes. The response of the camera is stable under filtering even for pixel values with an SNR of 1 or smaller. Notice, that the dark-current-noise of the camera is Gaussian with standard deviation 3. The discrete nature of the photo and electron shot-noise completely cancels out when multiple pixels are combined by filtering. The spectral calibration of our system means straightforwardly taking images of a white diffuse reference surface under the known LED illumination and dividing the response by the LED spectrum. The resulting sensitivity for each wavelength band can be taken from Figure 3. Finally, we checked the complete calibration of both types of cameras by a cross-validation experiment. This is done by simulating the RGB response to an X-Rite colorchecker passport from a spectral image taken with the spectral camera system. This way all calibration results are combined. The simulated RGB response matches the real response extremely well which is shown in Figure 4.

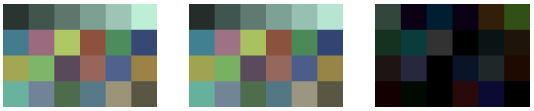

(a) Real RGB data (b) Simulated RGB data (c) Difference ×10

Figure 4: Cross validation of the spectral calibration: (a) real response of RGB cameras to color checker fields, (b) simulation of responses by applying the RGB filter matrix **C** to a spectral image captured using the spectral camera system, (c) 10× scaled difference image showing that our calibration used to generate the image in (b) is very exact.

5 EVALUATION

Prerequisites. For the evaluation of our method, we used four challenging datasets: a red fabric made of four different yarns, a collection of colorful Lego bricks, a hand-made color checker with diffuse and specular fields and a wallpaper having an embossed structure. For all of these samples, complete spectral ground truth data is available that was captured with a gonioreflectometer setup (Rump et al., 2010).

Simulated Data. To evaluate the reconstruction quality achievable by our method, we first performed simulations based on spectral ground truth data. This is extremely helpful because a pixel-wise comparison between reference and reconstruction can be made. This is not easily possible when using real data since the geometries and resolutions of the setup used for the ground truth measurements and the setup described in Section 4 are quite different. Furthermore, a basic understanding about the method and its properties can be gained without having too much bias by real-world data.

To have a scenario as realistic as possible, we performed a detailed simulation of the capture process. For the image capture in the CCD cameras the calibration results from Section 4 are used. The below equation describes how a pixel value I is generated from an incident irradiance x and exposure time t by means of the camera mapping $g : \mathbb{R} \to \mathbb{N}$:

$$I = g(x,t) := \lfloor f^{-1}(x \cdot t \cdot Q_\lambda) + \Delta_{ADC} + N_\sigma \rfloor \qquad (5)$$

The I still has to be clamped to the valid range of pixel values, in the case of our cameras to 10 bit unsigned integers. Q_λ denotes the combined quantum efficiency of optical system and sensor at wavelength λ and f^{-1} is the OECF i.e. the inverse of the response function. Δ_{ADC} is the ADC offset of the camera and N_σ a random value drawn from a normal distribution with standard deviation σ mimicking the various noise sources inside of the capture process. It is a simplifying assumption to model the effect of the different capturing noise sources as Gaussian noise N_σ. However, this simplification is to some extend justified by the varying nature of the different noise components. The values for f, Q, Δ_{ADC} and σ are taken from the calibration described in Section 4. We therefore end up with a detailed simulation of our measurement setup that helps us to evaluate the quality of spectral reconstruction in dependence on the different parameters.

Starting with a spectral reference image S_{ref} and the spectral power distribution L of the illumination, we first simulate an exposure series for the RGB images by computing $I_{RGB}(p) = g(\mathbf{C}S_{ref}(p)diag(L),t_i)$ for all pixels p of the reference image S_{ref} and for different exposure times t_i. The RGB-LDR images are recombined to form HDR images using Robertson's algorithm (Robertson et al., 2003). For the spectral images, one single exposure per wavelength band is simulated by computing $I_{spectral}(p) = g(S_{ref}(p)diag(L),t_\lambda)$.

During our experiments, it turned out to be the best solution to use 4 different exposures t_i for the RGB cameras. For the spectral camera, we calculated the exposure time according to equation 2. That is, we accept more noise in those spectral bands having bad support from light source and quantum efficiency. The size of the Gaussian filters in the reconstruction has to be adjusted accordingly.

Our simulation helps to choose good values for the capture and reconstruction parameters in beforehand. In Figure 3, we show the exposure times t_λ for the spectral camera system and the filter sizes of the gaussian filters in the reconstruction process. The standard deviation σ for the Gaussians was then set to $1/5$ of the filter size.

Full Correspondences. In many simple use cases, just one spectral image needs to be taken. In this case, the input to the reconstruction algorithm is a high quality RGB image and all the band-filtered images corresponding to the wavebands of the spectral camera (in our case 32, ranging from 410 to 720nm in 10nm steps). We used one image (texture) per example material as reference image. After running our new algorithm, the result S is compared to the reference image S_{ref}.

Figure 5 shows that our method successfully recovers spectral images that are very close to the ground truth. We selected representative spectra by picking both points with low and high RMSE in the color mapped (Green, 2011) error maps. The highest errors for the wallpaper material can be found in spectra (4 – 6). The deviations occur mostly in the very

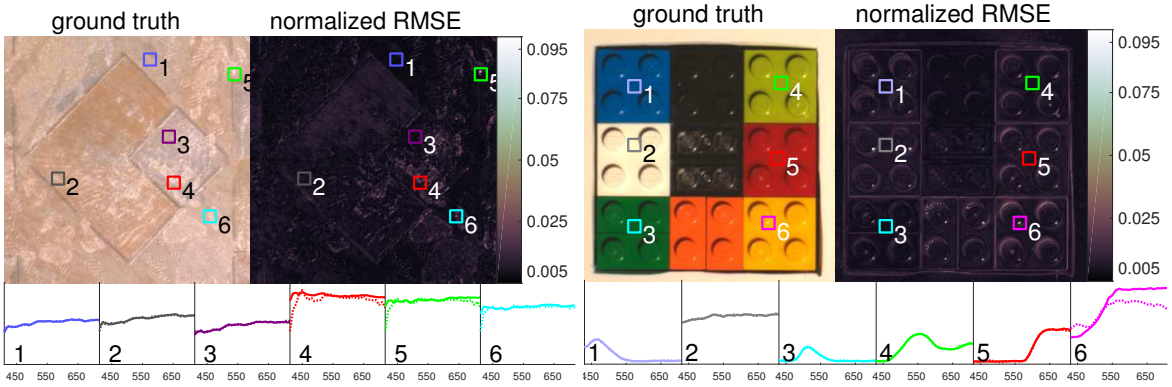

(a) Wallpaper (b) Lego

Figure 5: Normalized RMSE map of reconstructions of single images selected from two materials: shown respectively on the left is the ground truth image (converted to RGB for display), whereas the right hand side shows an error map of the RMSE of the reconstruction obtained from our simulated, artificially corrupted data. The pixel-wise RMSE is normalized by the mean over all pixel intensities of the ground truth spectral image. Inset below are some representative ground truth (solid) and reconstruction (dotted) spectra. Due to limited space, we omitted the reconstructed images as there is no noticable difference in comparison with the ground truth when converted to RGB.

blue and red bands, which are the ones with the highest noise levels. For the vast majority of the pixels, the two spectra are virtually indistinguishable. For the Lego material, only spectrum (6) shows significant deviations from the ground truth. This error occurred in a highlight, which has a dramatically different spectrum than the surrounding. We discuss these errors in more detail in Section 6.

Sparsely Measured Spectral Bands. Reconstructing multiple images at once is the much more challenging case. Here, we aim at providing only one noisy monochrome image per spectral band and spread this information over several RGB images. Even though there is no RGB image having complete spectral information, the regularization helps to share the information between the images. In this way, the exposure time for the spectral camera system is kept minimal and the spectral information can be acquired simultaneously with the RGB data. Using this approach, spectral imaging can be accelerated to the speed of RGB imaging and – in our use case – the capture of spectral reflectance can be performed at the speed of established RGB devices.

For our tests we capture 10 HDR RGB images while acquiring all of the 32 noisy, band-filtered images, as we are able to achieve exactly these numbers with our setup. Since the spectral camera is mounted at 45° elevation angle, we use only RGB images and the corresponding noisy spectral data from this elevation. Additionally, we added 10 RGB images without any spectral information and with different elevation angles. This way, complete bi-angular reflectance can be reconstructed using our method.

In Figure 6, error maps of the normalized RMSE are shown. Figure 7 displays histograms that show the cumulative behaviour over the entire experiments, i.e. over all pixels of all the twenty images per material. Both figures indicate that – just as in the single image case – the errors are concentrated at low values, showing the high quality of the reconstruction. The bin counts in the histograms of Figure 7 slightly increase for the images captured at different elevation angles than the one where the spectral camera was placed. However, these increased errors are negligible considering the logarithmic scaling of the y-axis. In the textures of Figures 5 and 6 there is no noticable increase of the errors from the "known" images to the "unknown" ones, which indicates that parallax effects have no large impact on the reconstruction quality. Therefore, high-quality spectral reflectance can be captured at high speed using our method.

Real Data. To test our algorithm on real data, we captured reference data for an X-Rite colorchecker passport with our spectral camera system using a total exposure time of 226212ms. Subsequently, we captured RGB and noisy band-filtered images with a total exposure time of 7463ms and performed a reconstruction using our novel algorithm. Figure 8 shows a comparison between reference and reconstructed spectra for some of the color fields. The figure shows that our algorithm achieves nearly the same results as the reference capture while requiring exposure times that are about 1.5 orders of magnitude smaller. There are again some more erroneous reconstructions at the boundaries of the checker fields, which result from gloss in these pixels and potentially a slight misalign-

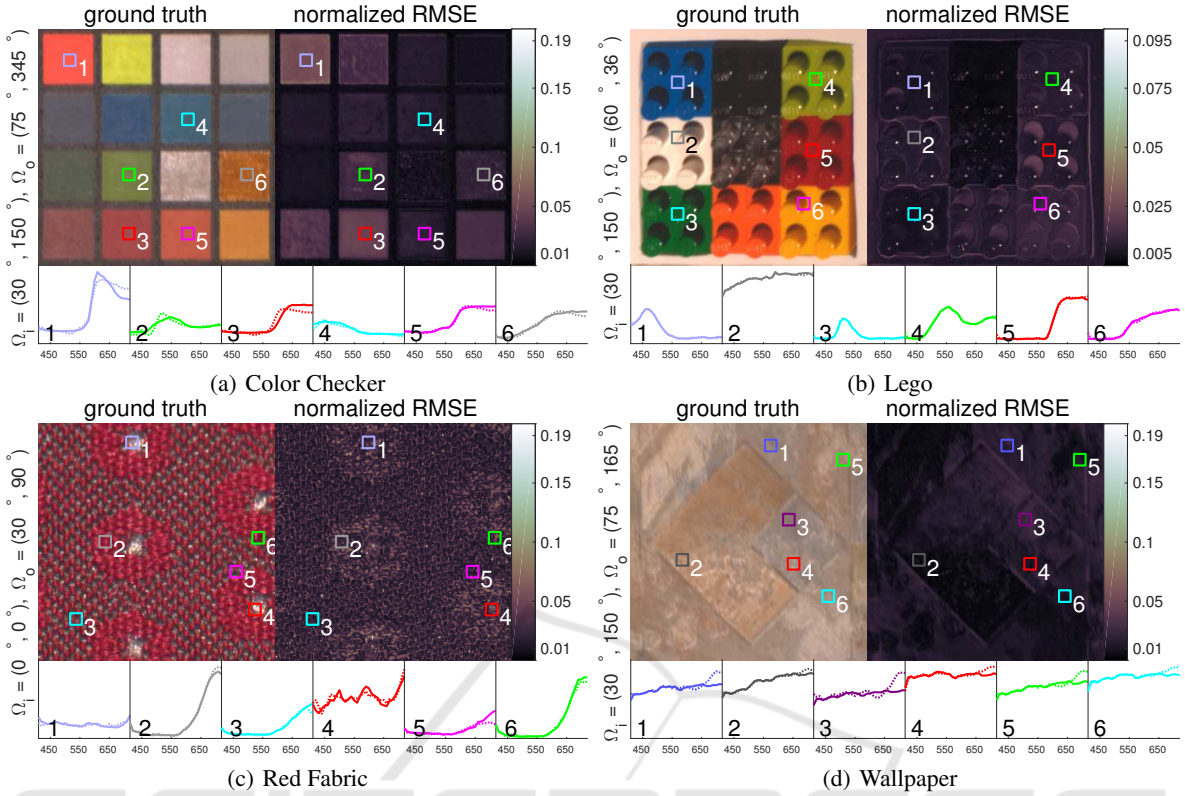

Figure 6: Normalized RMSE maps for all of the four tested materials: We selected representative textures from elevations (indicated respectively on the left as the first of the two angles of Ω_o) different than the 45° where we captured the band-filtered images. Shown respectively on the left is the ground truth image (converted to RGB for display), whereas the right hand side shows an error map of the RMSE of the reconstruction obtained from our simulated, artificially corrupted data. The pixel-wise RMSE is normalized by the mean over all pixel intensities of the ground truth spectral image (notice the different scaling of the colormap of the Lego material). Inset below are some representative ground truth (solid) and reconstruction (dotted) spectra. Due to limited space, we omitted the reconstructed images as there is no noticable difference in comparison with the ground truth when converted to RGB.

ment of the spectral bands and the RGB images.

6 LIMITATIONS

The reconstruction quality of our method depends directly on how much the regularization biases the result. Since it is assumed that similar RGB values have similar spectra, scenes containing two or more metamers may pose problems. Especially for reflectance capture, metamers may only occur for certain azimuth angles, if anisotropic materials are present. However, we consider the metamerism problem to be an extremely rare case and in our tests this problem did not occur. Moreover, the problem can be circumvented in many cases by adding spatial proximity information to the appearance space projection to distinguish between metamers that are not spatially adjacent. Another limitation is the occurrence of Fresnel reflections at certain elevation angles. These reflections show both spectral and angular dependence, as the refractive indices of material layers vary with the wavelength. The assumption that spectral data from only one elevation can be propagated to the entire hemisphere can thus be violated by some material classes. This limitation can, however, easily be handled by addition of one or more spectral cameras at different elevations.

Furthermore, the convergence speed of the spectral recovery directly depends on the size of the Gaussian filters used to get rid of the noise in the band-filtered images. In effect, this limits the size of the filters and this way the acceptable noise level resulting in a lower bound on the acceptable exposure times for the spectral camera system. Of course, this problem can be circumvented if a better optimization scheme is used.

The last limitation arises from the proposed setup only. Since we integrated only one spectral camera at

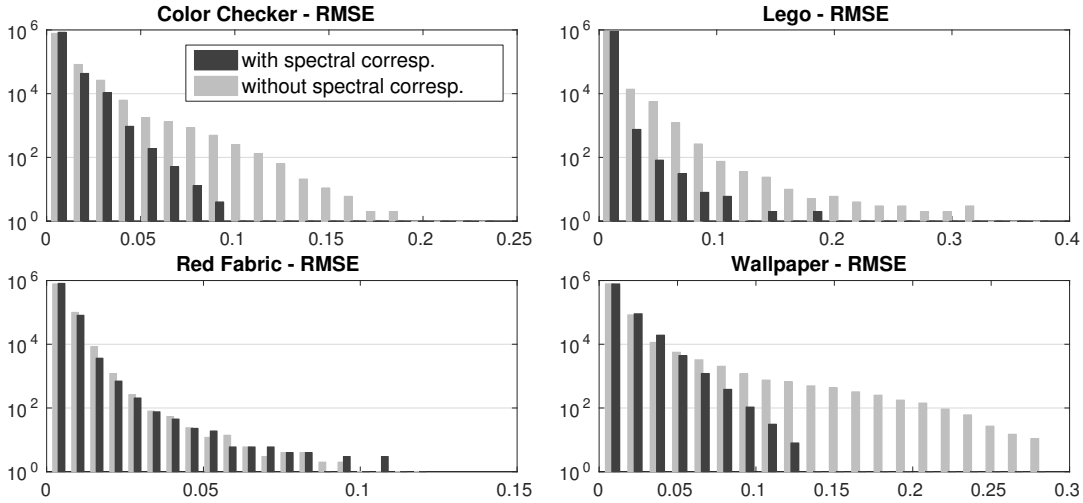

Figure 7: RMSE histograms for all of the four tested materials: For each of the four materials we compute a pixel-wise RMSE over all the 32 channels. We separated the first ten images, which were measured at the 45° elevation of the spectral camera, from the remaining ten images where no spectral bands with pixel correspondences where acquired. In total, most of the errors are close to zero with only a very small fraction of the pixels above an RMSE of ~ 0.03 (notice the logarithmic scale of the y-axis). As expected there is a noticable increase of the histogram counts for higher RMSEs for the images without direct spectral correspondences. However, this increase occurs for a very small fraction of the pixels and is therefore perceptually virtually unnoticeable, as can be seen in the other figures.

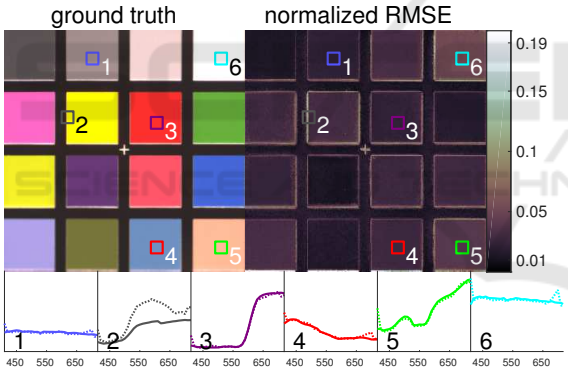

Figure 8: Spectral reconstruction using real data: the left part shows the RGB-converted ground truth data, the right part the normalized RMSE between the reference and our reconstruction. The reference data (solid plots) was obtained using long exposure times and required a total exposure time of 226212ms. The reconstruction by our algorithm was based on shots with a total exposure time of 7463ms. The result indicates the robustness of our reconstruction against high noise levels. Spectral imaging is accelerated by about 1.5 orders of magnitude.

45° elevation angle, materials showing dependence of spectra on angle – like materials having interference effects – cannot be reconstructed well. This, however, could be easily fixed by adding additional spectral cameras.

7 CONCLUSIONS

In this paper, we presented a novel method for spectral imaging, especially suited for the capture of multiple spectral images at once. Our method reconstructs spectral images from high-quality RGB and noisy band-filtered images using a novel variant of the *spectralization* method. We have proven the stability and quality of the method using both simulated and real data. Due to the stability of our reconstruction against noise in the band-filtered data, taking spectral images can be vastly sped up. This way, spectral imaging at the speed of RGB imaging is possible.

In general, our method is not limited to specialized hardware like the RGB measurement device we used to generate the data for our experiments. As long as a reasonably good registration of RGB and spectral images is available, e.g. by using a beam splitter, our approach can be applied to reconstruct the spectral data cube for one or multiple RGB images. Another potential application would be the capturing of spectral video. Here the only constraint is to capture enough spectral band frames before the scene changes considerably. The alignment between RGB and spectral bands could be achieved with optical flow.

It should be noted that in the context of material measurements there are certain constraints on the positioning of RGB and spectral cameras. To avoid parallax effects that arise as soon as materials are imaged that are not perfectly flat, the optical paths for

RGB and spectral cameras should match as closely as possible. This can either be achieved by using a beam splitter or by a similar setup like ours, where the separation of the cameras matches exactly the angular sampling of the material. Our approach should also be applicable to image-based reflectance measurement like the one developed by Hullin et al. (Hullin et al., 2010). For the acquisition of HDR images, the authors' setup requires long measurement times with exposures of up to 16s. Here, our method could provide a significant speed-up by decoupling spectral and HDR acquisition using beam splitter optics, the existing combination of LCTF and monochrome camera, and an additional monochrome or RGB camera to acquire the HDR data.

In the future, it should be investigated whether the applied principle is applicable using even more levels of spectral resolution (e.g. monochrome, RGB, and band-filtered), accepting different SNRs at the different levels. Perhaps the presented method could even help to get faster RGB imagery in certain use cases since it can be straightforwardly applied to monochrome and noisy RGB images. Other snapshot spectral imaging techniques like CTIS could also be used to provide the low-resolution spectral input data as soon as the problem of spatially registering RGB and spectral data is solved. Furthermore, it would be helpful to have a better optimization scheme to allow for a faster reconstruction.

ACKNOWLEDGEMENTS

This work was funded by the German Science Foundation (DFG) under research grant KL 1142/7-1.

REFERENCES

Green, D. (2011). A colour scheme for the display of astronomical intensity images. *arXiv preprint arXiv:1108.5083*.

Hagen, N. and Kudenov, M. W. (2013). Review of snapshot spectral imaging technologies. *Optical Engineering*, 52(9):090901–090901.

Hardeberg, J. Y., Schmitt, F., and Brettel, H. (2002). Multispectral color image capture using a liquid crystal tunable filter. *Optical Engineering*, 40(10):2532–2548.

Hardeberg, J. Y., Schmitt, F., Brettel, H., Crettez, J.-P., and Maitre, H. (1999). Multispectral image acquisition and simulation of illuminant changes. In *Colour Imaging - Vision and Technology*, pages 145–164. Wiley.

Hullin, M. B., Hanika, J., Ajdin, B., Seidel, H.-P., Kautz, J., and Lensch, H. P. A. (2010). Acquisition and analysis of bispectral bidirectional reflectance and reradiation distribution functions. *ACM Trans. Graph. (Proc. SIGGRAPH 2010)*, 29(4):97:1–97:7.

Imai, F. H. and Berns, R. (1999). Spectral estimation using trichromatic digital cameras. In *Proceedings of the International Symposium on Multispectral Imaging and Color Reproduction*, pages 42–49.

Imai, F. H. and Berns, R. S. (1998). High-resolution multispectral image archives: A hybrid approach. *Proc. of the IS&T/SID Sixth Color Imaging Conference*, pages 224–227.

Krishnan, D. and Fergus, R. (2009). Dark flash photography. In *ACM Transactions on Graphics, SIGGRAPH 2009 Conference Proceedings*, volume 28.

Matsui, S., Okabe, T., Shimano, M., and Sato, Y. (2009). Image enhancement of low-light scenes with near-infrared flash images. In *Asian Conference on Computer Vision*, pages 213–223. Springer.

Petschnigg, G., Szeliski, R., Agrawala, M., Cohen, M., Hoppe, H., and Toyama, K. (2004). Digital photography with flash and no-flash image pairs. *ACM transactions on graphics (TOG)*, 23(3):664–672.

Robertson, M. A., Borman, S., and Stevenson, R. L. (2003). Estimation-theoretic approach to dynamic range enhancement using multiple exposures. *Journal of Electronic Imaging*, 12(2):219–228.

Rump, M. and Klein, R. (2010). Spectralization: Reconstructing spectra from sparse data. In *SR '10 Rendering Techniques*, pages 1347–1354, Saarbruecken, Germany. Eurographics Association.

Rump, M., Sarlette, R., and Klein, R. (2010). Groundtruth data for multispectral bidirectional texture functions. In *CGIV 2010*, pages 326–330. Society for Imaging Science and Technology.

Rump, M., Zinke, A., and Klein, R. (2011). Practical spectral characterization of trichromatic cameras. *ACM Trans. Graph.*, 30(6).

Schwartz, C., Sarlette, R., Weinmann, M., Rump, M., and Klein, R. (2014). Design and implementation of practical bidirectional texture function measurement devices focusing on the developments at the university of bonn. *Sensors*, 14(5).

Shrestha, R. and Hardeberg, J. Y. (2014). Evaluation and comparison of multispectral imaging systems. In *Color and Imaging Conference*, volume 2014, pages 107–112. Society for Imaging Science and Technology.

Takeuchi, K., Tanaka, M., and Okutomi, M. (2013). Low-light scene color imaging based on luminance estimation from near-infrared flash image. In *Proceedings of IEEE International Workshop on Computational Cameras and Displays (formerly PROCAMS)(CCD/PROCAMS2013)*, pages 1–8.

Tsuchida, M., Arai, H., Nishiko, M., Sakaguchi, Y., Uchiyama, T., Yamaguchi, M., Haneishi, H., and Ohyama, N. (2005). Development of BRDF and BTF measurement and computer-aided design systems based on multispectral imaging. In *Proc. AIC Colour 05 – 10th congress of the international colour association*, pages 129–132.